ChemComm

HIGHLIGHT

View Article Online
View Journal | View Issue

Cite this: *Chem. Commun.*, 2025, **61**, 11538

Long-range electron transport in self-assembled fibrils of peptides rich in aromatic residues

Ramesh Y. Adhikari

Understanding the mechanism of charge transport in proteins and peptides in physiologically relevant environments has been a long-standing interest, as several physiological processes involve ion and electron transfer in proteins. This has attracted the interest of researchers working on biomolecular electronics. However, the discovery that some bacteria can produce proteinaceous nanowires capable of transporting electrons over distances of up to the centimeter range has opened a new paradigm for the development of synthetic biomimetic proteinaceous nanowires as electronic materials. Inspired by the structural models suggesting that closely packed aromatic residues facilitate charge transport through proteinaceous nanowires generated by these bacteria, various groups have developed synthetic peptide-based nanofibrils that allow long-range electron transport along their lengths. This highlight reviews recent developments in the construction and characterization of self-assembled fibrils of aromatic residue-rich peptides designed for long-range electron transport, outlines ongoing challenges, and lays out opportunities in the field. The ability to carry out efficient electron transport *via* self-assembled peptide nanofibrils and tune their electrical properties by modifying constituent peptide sequences would herald a new era of peptide-based solid-state electronics. This would also provide a sustainable bio-based alternative to current approaches in the development of electronic materials.

Received 24th May 2025,
Accepted 11th July 2025

DOI: 10.1039/d5cc02953h

rsc.li/chemcomm

Introduction

Proteins are an essential part of life, and the movement of electrons within proteins enables physiological processes related to biological energy conversion and storage. Such movement of electrons through proteins is termed the electron transfer (ET) process.[1,2] In this process, electrons are shuttled through closely packed redox-active sites due to the redox potential difference between donor and acceptor units. This transport within proteins is possible due to electrostatic screening provided by ions in the electrolyte solution that completely or partially surround the protein. Electron transfer in such systems can occur over distances of a few nanometers, which is sufficient to enable biological processes like respiration, photosynthesis, and hydrogenases.[1]

While such electron transfer in proteins for physiological processes is well-known, the developments in the field of molecular electronics gave rise to the idea of whether some of these proteins can be used as conducting units in molecular electronics.[1,3,4] The biological ET process in proteins can be probed by spectroscopic and electrochemical techniques, where the proteins are exposed to the solution environment. However, to study the feasibility of using these molecules for solid-state electronics, they need to be removed from the solution environment and placed between electrodes. Electron shuttling *via* protein in such situations occurs due to the potential difference applied between the contact electrodes rather than the difference in the chemical potential of electrons in different regions within the proteins. Such a process is called electron transport (ETp)[1] which follows mechanisms such as

Department of Physics and Astronomy, Colgate University, 13 Oak Dr, Hamilton, NY 13346, USA. E-mail: radhikari@colgate.edu

Ramesh Y. Adhikari

Ramesh Adhikari is an assistant professor in the Department of Physics & Astronomy at Colgate University, USA. He received his PhD in physics from the University of Massachusetts Amherst, where he studied charge transport in microbial nanowires. He has extensive experience in electrical and surface characterization of nanomaterials. He is also passionate about undergraduate education and research. His lab focuses on the development of bio-based materials for electronics. Current research problems in his lab include the development of leaf-based electronics and peptide materials for electronic applications.

thermally activated hopping, sequential tunnelling, superexchange, or flickering tunnelling.[1,5]

Historically, a large number of studies conducted to understand electron transport in proteins have been the ones with redox centres such as cytochrome and azurin. Electron transport in these systems is limited to distances of up to a few nanometers.[2,6] The conduction in these systems declines exponentially as a function of their lengths[7] albeit these molecules demonstrate higher conduction compared to molecular wires at lengths over 7 nm.[2,7] More recently, it has also been demonstrated that globular proteins lacking redox-active centres can also allow for electron transport.[8–10] While the conduction at this length scale makes these molecules strong candidates for molecular electronics, it limits their wider application in mesoscale electronics, where the electrons may have to be channelled over distances of hundreds of nanometres to a few micrometres.

The discoveries that various bacteria can generate conducting proteinaceous microbial nanowires that can transport electrons over distances ranging from a few micrometres to even centimetre scale have led researchers to realize that, under certain conditions, proteinaceous filamentous structures can facilitate long-distance electron transport. For instance, the bacterium *Shewanella oneidensis* develops nanowires composed of multiheme c-type cytochromes, which act as redox cofactors for making long-range charge transport possible.[11] The transport along the length of these nanowires, which are outer membrane and periplasmic extensions of the bacteria,[12] could occur over a micrometre range and can be tuned by a transverse electric field.[13] The electron shuttling along the length of these nanowires is attributed to thermally activated hopping transport facilitated by closely packed cytochromes.[14] More recently, it has been reported that multicellular Cable bacteria, found in marine and freshwater sediments, possess periplasmic filaments composed of metalloproteins with nickel-based cofactors[15] and can transport electrons to distances of over a centimeter.[16] Electron transport in this system is mediated by those cofactors and attributed to thermally activated multistep hopping transport at higher temperatures (>75 K) and electron tunnelling assisted by quantized vibrational modes at lower temperatures.[17]

Geobacter sulfurreducens,[18] one of the most commonly studied metal-reducing bacteria, and its related species *Geobacter metallireducens*[19] can produce conductive proteinaceous nanowires that can be a few nanometres in diameter and up to a few micrometres in length, resulting in a high aspect ratio.[20] The composition of these nanowires and the mechanism of electron transport in them have been topics of vigorous debate. Over the years, two major categories of conducting nanowires in *G. sulfurreducens* have been identified[21] – α-helical PilA protein-based homopolymer filament called pili (or e-pili due to their conductive nature)[22,23] (Fig. 1a) and multiheme cytochrome-based OmcS,[24] OmcZ,[25,26] and OmcE[27] nanowires (Fig. 1b–d). There is a debate over whether electron transport in pili nanowires is due to delocalized transport resulting from closely packed aromatic amino acid residues[28,29] or hopping transport mediated by those aromatic amino acids.[30,31] The electron transport in the cytochrome-based nanowires is attributed to hopping transport mediated by closely stacked hemes associated with the cytochromes.[24,25]

Over the years, it has been reported that a wide range of phylogenetically diverse sets of bacteria can generate conductive nanowires, which could either be composed of the PilA protein[32] or multiheme cytochromes.[33] These discoveries of not only the existence of naturally designed conducting proteinaceous nanowires but also their pervasive prevalence in the microbial world are quite exciting since proteins are generally believed to be insulators.[9]

One of the limiting factors in the widespread use of *G. sulfurreducens* e-pili is the difficulty in scaling up pili production due to limitations in bacterial growth rate and the purification process necessary to separate nanowires from the rest of the bacteria. To overcome that bottleneck, pili genes from *G. sulfurreducens* can be introduced to *Escherichia coli*, which can multiply at a much faster rate and therefore allow for large volume production of pili.[34] This process would still require one to undergo microbial growth, pili extraction, and a purification process. An alternative method that can be employed could be synthesizing bioinspired proteins and peptide motifs *in vitro*, followed by their self-assembly to construct fibrillar structures with the desired electronic properties. The self-assembly route facilitates scaling up production and also reduces the barriers to conducting studies aimed at examining both the self-assembly mechanism and charge transport properties. Development of conducting peptide and protein-based structures would be of great interest to the field of electronic materials, as there is an increasing interest in bio-based and biocompatible materials for sustainable electronics and bioelectronics.[35]

Inspired by the idea that conducting nanowires produced by some bacteria can be composed of cytochromes, development of various biomimetic synthetic cytochrome-based conducting nanowires has been reported.[36–38] Altamura *et al.* constructed electron-conducting nanowires by inserting metalloprotein rubredoxin, which has iron as a redox centre, within the nanofibers of self-assembled non-conducting prion domain.[37] These nanowires had diameters that varied with pH of the solution, with approximately 8 nm at pH 4.5 and a length of approximately 12 μm. Chen *et al.*[38] demonstrated construction of conducting nanofibrils with metalloprotein multiheme c-type cytochromes as redox centres within self-assembled gamma-prefoldin (γPFD) protein filaments. These nanowires had a diameter of approximately 3 nm and a length exceeding 250 nm. Some proteins have affinity towards metal units, allowing them to be attached to protein-based materials for enhancing electron transport.[39–41] Travaglini *et al.*[36] took advantage of the affinity of the coiled-coil domain of γPFD molecules towards heme groups to incorporate heme within γPFD filaments, as had been done with protein-based bulk materials,[40] to create conducting proteinaceous nanowires of diameters of about 9 nm and a length of over 1 μm.

On the other hand, influenced by the idea that *G. sulfurreducens* can produce conducting pili entirely composed of amino

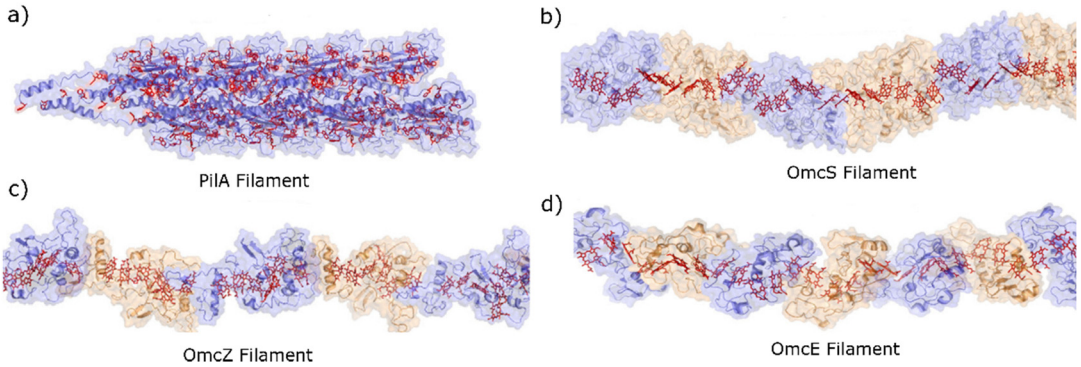

Fig. 1 Structural representation of various nanowires generated by bacteria *G. sulfurreducens* based on their composition. (a) PilA-based, and cytochrome-based (b) OmcS, (c) OmcZ, and (d) OmcE filaments. Aromatic residues in PilA filament and redox sites in cytochrome-based filaments are highlighted in red.[47] Reprinted with permission from N. Amdursky, *Current Opinion in Electrochemistry*, 2024, **47**, 101551. Copyright 2024 Elsevier.

acids, and that the electron transport in such nanowires relies on the close packing of the residues of aromatic amino acids, various groups have also reported the development of self-assembled, bioinspired synthetic peptides rich in aromatic residues that can form fibrillar structures through self-assembly and facilitate electron transport along their lengths. While engineered protein-based nanowires rich in metalloproteins as redox centres are interesting candidates for conducting nanowires for electronics, this highlight will focus on recent works on the development of these redox centre-deficient aromatic amino acid-rich conducting structures.

As in the case of proteins and peptides in their physiological environments, self-assembled peptide fibrils also allow for electron, proton,[42–44] and mixed proton-electron transport.[45] In this highlight, I will limit my discussion to reports of aromatic amino acid-rich peptide nanofibrils that are explicitly designed to promote electron transport along their length and outline the current state. For readers who are interested in learning about the mechanism of charge transport in short and long molecular wires of peptides, I recommend the 2015 review by Amdursky *et al.*[2] and a more recent review by Jang *et al.*[46] For those interested in a general overview of electron (and proton) transport in protein-based systems, readers may find a recent review by Amdursky[47] helpful. A short review[7] by Lindsay provides a good overview of electron transport in proteins. Those interested in a detailed discussion on theoretical models and experimental evidence of long-range electron transport in various protein-based materials would find the review paper by Ing *et al.*[5] useful.

Electron transport measurements in aromatic amino acid-rich fibrils

Individual aromatic amino acids and peptides rich in aromatic amino acids can self-assemble in various structures[48–52] due to π–π interaction between the aromatic residues, hydrogen bonding, and electrostatic interaction among amino acids, and also between amino acids and the surroundings. Fibrillar structures of aromatic amino acids and peptides rich in aromatic amino acid residues can be constructed *via* self-assembly in both solution environments[53–55] and vapor phase.[56,57] Over the years, various aromatic amino acid-rich biomimetic peptides, such as those inspired by biological amyloids, have been self-assembled and studied for their interesting chemical, mechanical, and optical properties.[53,58–60]

Inspired by the idea that long-range electron transport in *G. sulfurreducens* e-pili is facilitated by aromatic residues associated with aromatic amino acids of constituent peptides, in 2015, Creasey *et al.*[61] synthesized a bioinspired peptide with the sequence GFPRFAGFP (Fig. 2a) based on the proteins found in elastin and collagen. The peptide was designed for two major purposes: to achieve a helical structure that facilitates quasi one-dimensional self-assembly in solution, and to leverage the high abundance of aromatic amino acid phenylalanine (F) for intermolecular coupling during self-assembly, enabling π–π conjugation for constructing an electron transport pathway. The self-assembly of peptides into fibrils was carried out by preparing the peptide solution in water at a concentration of 10 mg mL^{-1}, followed by incubation at 37 °C for a duration of overnight to 7 days before proceeding with physical, chemical, and electrical characterizations.

When the incubated solution was drop-cast on a mica substrate and the AFM imaging was carried out, it was observed that the most prevalent features were fibrillar structures with lengths of up to 10 μm and diameters of about 0.5 nm (Fig. 2b), demonstrating the ability of the designed peptide to undergo quasi one-dimensional self-assembly. For electrical characterization, two two-terminal conductivity measurement setups were prepared by placing two molybdenum plates onto the substrate with the film of self-assembled fibril network. The resulting current–voltage (*I–V*) curve was linear within the applied voltage range of 2 V to −2 V (Fig. 1c). The conductance of the fibril network was in the range of 10^{-11} to 10^{-10} S. This value was higher than the value for non-incubated sample, where the self-assembly process was limited due to lack of enough time for peptide units to assemble and therefore prevented the peptide from undergo the formation of long fibrils. Fluorescence spectroscopy suggested the presence of π–π interactions, implying that these interactions may be

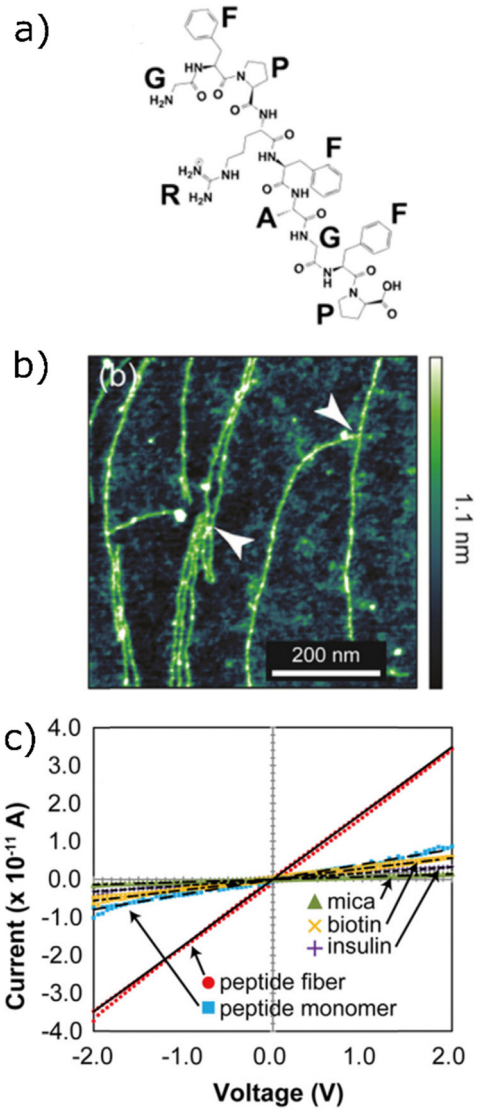

Fig. 2 (a) Chemical structure of the peptide used for the construction of self-assembled fibrils for this study. (b) AFM topography images of self-assembled fibrils. (c) Current–voltage (*I–V*) response of peptide fibril network (red) compared to the response from the peptide before incubation (blue) and other biomolecules such as insulin (purple), biotin (yellow) as well as background response from mica substrate (green).[61] Reprinted with permission from R. C. G. Creasey, Y. Shingaya and T. Nakayama, *Materials Chemistry and Physics*, 2015, **158**, 52–59. Copyright 2015 Elsevier.

responsible for the formation of long fibrils that allow for electron transport along their lengths.

Inspired again by the idea that aromatic amino acids in *G. sulfurreducens* pili are responsible for making electron transport possible, Ing *et al.*[62] reported charge transport studies in self-assembled fibrils of peptide Ac-ELKAIAQEFKAIAKEFKA IAF^{I}EFKAIAQK-NH_2 (here, F^{I} represents iodo-phenylalanine).[63] The peptide that forms a helical structure (Fig. 3a) had its sequence capped with glutamic acid (E) and lysine (K) to induce electrostatic interactions at the ends of the peptides and promote the formation of elongated fibrils during the self-assembly process. The self-assembly of the peptides into fibrils was then carried out by dissolving them in phosphate-buffered saline (PBS) solution. During the self-assembly process, the helical structures of peptides aggregated into an antiparallel coiled-coil hexamer (ACC-Hex, Fig. 3b) in a manner similar to how *G. sulfurreducens* pili are formed.[28] AFM images showed the formation of fibrils that were several micrometres in length and had diameters of more than 2 nm (Fig. 3c and d). The fibrils were then drop-cast onto interdigitated electrodes with a 5-μm spacing and left to dry before performing current–voltage (*I–V*) measurements.

The fibril network bridging the interdigitated electrodes had an average resistance of 188 ± 36 Ω with significantly higher conductance for the fibril network (Fig. 3e) compared to the dried buffer control and amyloid-β (Aβ) fibres (mentioned later). Based on the single fibril measurements, the conductivity of these fibrils was found to be 1.12 ± 0.77 S cm^{-1}, which is about two orders of magnitude larger than the wild-type *G. sulfurreducens* pili in a physiologically relevant pH of 7 with the conductivity of 0.051 ± 0.011 S cm^{-1} and an order of magnitude higher compared to the pili in pH 2 with conductivity of 0.188 ± 0.034 S cm^{-1}.[18] Biopotentiostat cyclic voltammetry on ACC-Hex nanofibers demonstrated that the current through the nanofiber is independent of gate potential (V_S) but depends only on the source–drain (V_{DS}) potential (Fig. 3f), a behaviour similar to the systems with band-like charge carrier conduction. They also observed that the conductance increases with decreasing temperature (Fig. 3g), another behaviour similar to systems with band-like conduction and unlike thermally activated hopping.

For control measurements, the authors prepared self-assembled amyloid beta (Aβ) fibrils[64] constructed from Aβ 1–40 peptide, which also contains aligned aromatic residues. Self-assembled Aβ fibrils had the same aspect ratio as that of ACC-Hex fibrils. However, the Aβ fibril network demonstrated an average resistance of 1.0 × 10^{8} Ω, which is several orders of magnitude larger than the resistance of the ACC-Hex fibril network. With this observation, in conjunction with the crystallographic data for the ACC-Hex, according to which the aromatic amino acid residues have larger spacing and off-angle packing to allow for a continuous π-stacking chain along the length of the filament, the authors conclude that aromatic amino acids stacking may not be necessary for long range electron transport in peptide fibrils. While ACC-Hex fibrils are composed of α-helical building blocks, Aβ fibrils are composed of building blocks with β-sheets. The authors suggest that it is possibly the helical backbone of the peptides that is important in facilitating long-range electron transport. Despite the presence of aromatic residues, much lower conduction in Aβ fibrils was attributed to the lack of α-helical building blocks that would have minimized the energetic barrier for charge transport across short homopeptides.

Inspired by the aforementioned potential role of aromatic residues, α-helices, and coiled-coil structures in the promotion of electron transport along self-assembled peptide fibrils, in 2019, Creasey *et al.* again reported the construction of two types of synthetic peptides with 21 amino acids in the sequence.[65]

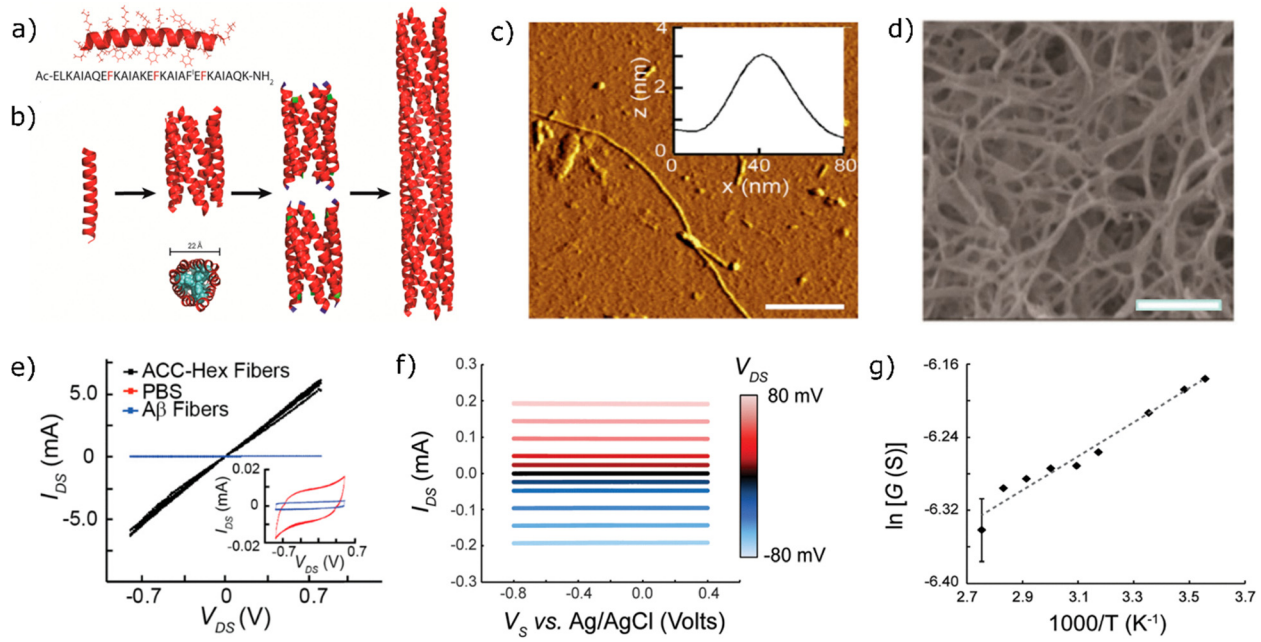

Fig. 3 (a) Crystal structure and sequence of the peptide used for this study. (b) Scheme of peptide fibril formation mechanism. Multiple helical structures come together to form a coiled-coil hexamer (ACC-Hex) with a diameter of about 22 Å. These hexamers stack end-to-end due to electrostatic interaction between glutamic acid (green) and amide lysines (blue) at their terminals to form fibrils. (c) Topographical AFM image of the self-assembled peptide fibrils. The inset shows that the diameter of the fibril is slightly more than 2 nm (scale bar: 500 nm). (d) SEM image of ACC-Hex nanofibers (scale bar: 500 nm). (e) Current voltage (I–V) response of the ACC-Hex fibrils compared to amyloid beta fibrils (Aβ fibrils) and phosphate buffered saline (PBS). (f) Drain–source current (I_{DS}) for changing drain–source voltage (V_{DS}) as a function of reference electrode voltage (V_S) acting as gate. (g) Average drain–source conductance (G) as a function of changing temperature.[62] Reprinted with permission from N. L. Ing, R. K. Spencer, S. H. Luong, H. D. Nguyen and A. I. Hochbaum, *ACS Nano*, 2018, **12**, 2652–2661. Copyright 2018 American Chemical Society.

Both peptides had an identical sequence of amino acids, except for those containing aromatic residues. Peptide labelled F6 had phenylalanine (F) at six different locations on the peptide sequence: Ac-FKEFAKLFKEFAKLFHEFAKL-NH_2 (Fig. 4a). The other peptide, labelled L6, had all phenylalanine in the previous sequence replaced with an aromatic residue deficient amino acid leucine (L): Ac-LKELAKLLKELAKLLHELAKL-NH2 (Fig. 4b). Both peptides were expected to form α-helical structures (Fig. 4c and d). The self-assembly of these peptides into fibrils was carried out by dissolving the peptides in water. Both peptides formed nano-fibrillar structures as observed in the AFM topographical images (Fig. 4e and f).

Electrical measurements on the fibrillar network were carried out by drop-casting peptide solution on indigitated

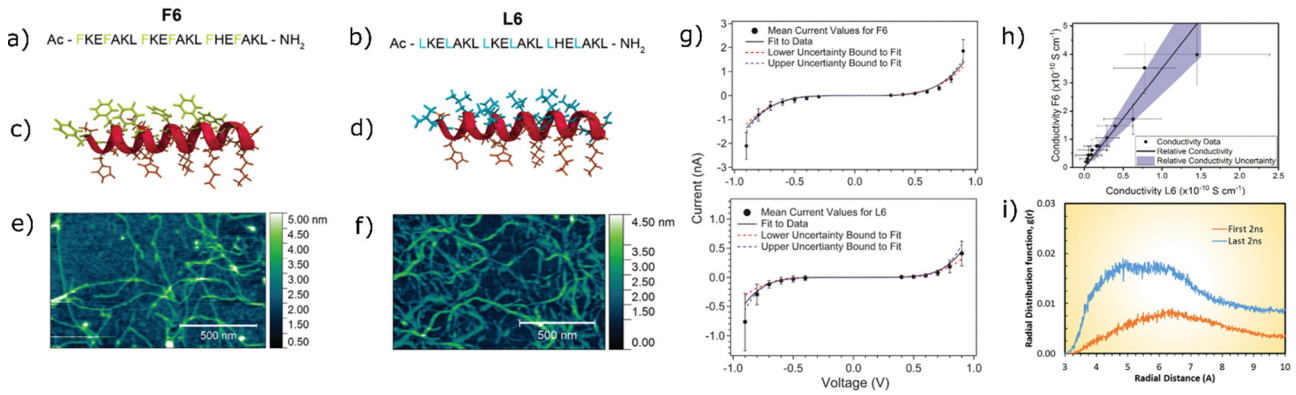

Fig. 4 (a) Sequence of the peptide rich in aromatic amino acid phenylalanine (F6) and (b) the same peptide with six aromatic units replaced by leucine (L6). Molecular structure of peptides (c) F6 and (d) L6. Topographical AFM image of self-assembled nanofibrils of (e) F6 and (f) L6. (g) Current–voltage (I–V) response of network films of F6 (top) and L6 (bottom). (h) Voltage dependent conductivity of F6 and L6 fibril network, where the solid lines indicate weighted mean values and the shaded area represents uncertainty around mean. (i) Distance between aromatic rings obtained from molecular dynamics simulations.[65] Used in accordance with Creative Commons public use license from R. C. G. Creasey, A. B. Mostert, A. Solemanifar, T. A. H. Nguyen, B. Virdis, S. Freguia and B. Laycock, *ACS Omega*, 2019, **4**, 1748–1756. Copyright 2019 American Chemical Society.

microelectrodes with an electrode gap of 5 μm. The resulting *I–V* curve (Fig. 4g) demonstrated that the F6 fibrils had a higher current response compared to L6 fibrils. Based on the overall weighted mean ratio calculation, it was determined that F6 was 3.5 ± 0.9 times more conductive than L6 (Fig. 4h). Radial distribution function based on the molecular dynamics simulation suggested that the aromatic residues of phenylalanine come closer together during the process of self-assembly, potentially allowing for improved electron transport (Fig. 4i).

While all these studies were inspired by the pilin structure of *G. sulfurreducens*, both in terms of helicity and presence of aromatic residues, the peptide sequences themselves were substantially different from those of the *G. sulfurreducens* PilA protein. Therefore, these studies did not exactly replicate the conduction mechanism or properties of *Geobacter* pili. In 2019, Cosert *et al.* synthetically constructed peptides with sequences analogous to that of *G. sulfurreducens* PilA nanowire with various lengths of truncations (Fig. 5a) at the amino-terminal (N-t).[66] These truncations reduced hydrophobicity and therefore increased the solubility of the peptide, and at the same time preserved the aromatic and charged amino acids essential for the formation of the nanowire structures (Fig. 5b). Among the peptides with 10, 19, 20, and 22 amino acid truncations, the one with 19 amino acid truncations at the N-t end ($PilA_{19}$) allowed for the highest cleavage efficiency and extraction and therefore, was used for further studies.

The self-assembly of $PilA_{19}$ resulted in the formation of the fibrils (Fig. 5c) comparable in their dimensions to the fibrils of native pili produced by *G. sulfurreducens* (Fig. 5d), which were used as a control. Conducting probe AFM (C-AFM) of the truncated pili fibril (Fig. 5e) demonstrated that the current response of the self-assembled fibrils was in the same range as that for the *G. sulfurreducens* PilA protein-based pili nanowires (Fig. 5f), with the average resistance within the same order of magnitude as well. Interestingly, the current–voltage (*I–V*) measurements of $PilA_{19}$ demonstrated less variation compared to similar measurements of PilA, which was attributed to the reduced aggregative nature of $PilA_{19}$, allowing fibrils to make better contact with the electrodes.

Contact resistance is an important parameter to consider when conduction measurements are carried out. All of the studies reported thus far involved two-probe measurements with fibrils being drop-cast on top of prefabricated electrodes. This introduces varying levels of contact resistance and therefore affects the reproducibility of measurements. Interestingly, Cosert *et al.* observed that chemical fixation used to improve contact between the fibrils and substrate did not demonstrate any substantial improvement over the conductance measurements over the fibrils without such chemical treatment. Such

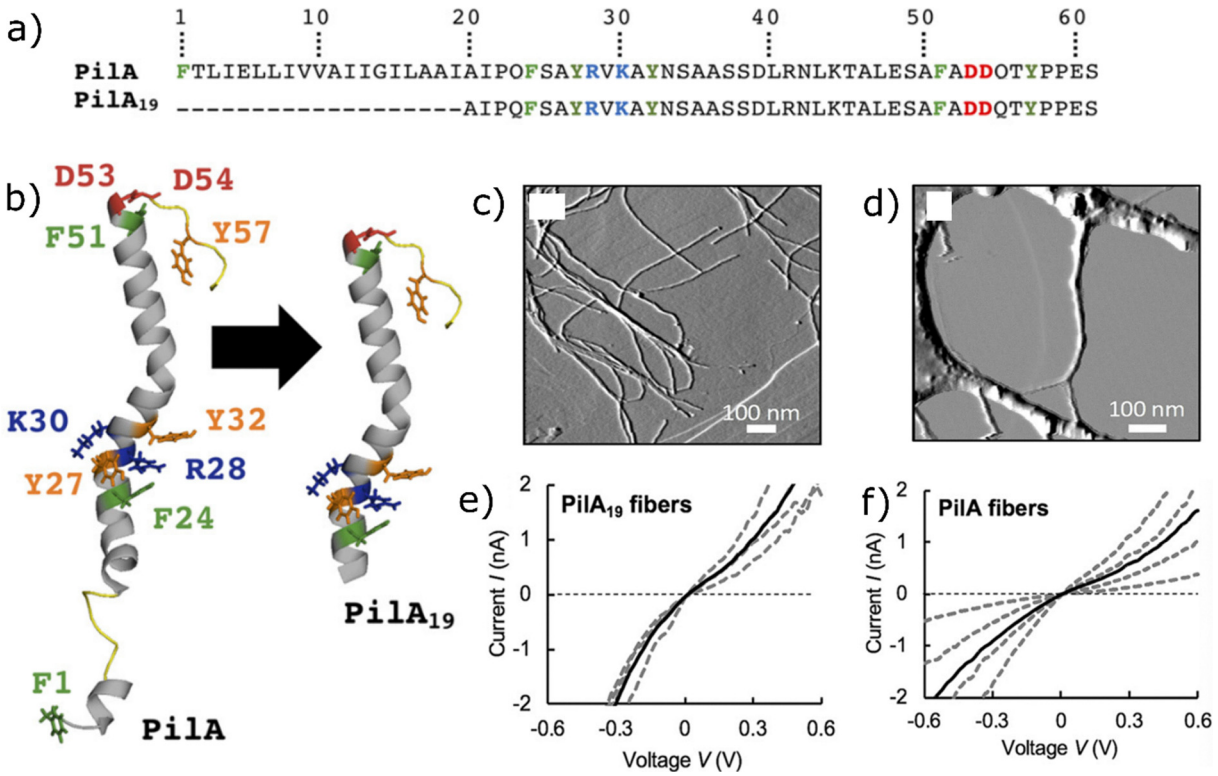

Fig. 5 (a) Amino acid sequence of PilA from *G. sulfurreducens* pili and its truncated counterpart $PilA_{19}$ obtained by removing 19 amino acids from PilA sequence. (b) Molecular structure of PilA and $PilA_{19}$. AFM amplitude image of (c) $PilA_{19}$ and (d) PilA nanofibrils. Current–voltage (*I–V*) response of (e) $PilA_{19}$ and (f) PilA nanofibrils measured with conducting probe AFM. Dashed lines represent individual measurements and solid lines are the average of four different measurements.[66] Used in accordance with Creative Commons Attribution 4.0 open access license from K. M. Cosert, A. Castro-Forero, R. J. Steidl, R. M. Worden and G. Reguera, *mBio*, DOI:10.1128/mBio.02721-19. Copyright 2019 Cosert *et al.*

situations could occur when the sample resistance (approximately 900 MΩ for $PilA_{19}$ fibrils[66]) is higher than the possible contact resistance between the sample and electrodes. Nevertheless, two-probe measurements do not allow for acquiring the intrinsic resistance of samples, required for calculating intrinsic transport properties such as conductivity, since the values will always include the contribution of contact resistance. In addition, most of the studies reporting self-assembled conducting fibrils of aromatic amino acid-rich peptides have been carried out in films of fibril networks. This introduces inter-fibril charge transfer resistance, which again limits the ability to understand the nature of intrinsic charge transport in a fibril.

To address these issues associated with contact between the fibrils and electrodes or neighbouring fibrils, Shipps *et al.* reported electrical measurements on individual self-assembled peptide fibrils using a four-point probe method in 2020.[67] For this purpose, they developed four different short peptides, two of which included tyrosine as the amino acid with aromatic residue, and two of the peptides had metal (Zn) linked to them. These peptides were labelled as (1) X1: Zn^{2+}NNQQNY; (2) X2: GNNQQNY (3) X3: Zn^{2+}GGVLVN; and (4) X4: KVQIINKKL (Fig. 6a). All of these short peptides formed amyloid microcrystal fibrils (Fig. 6b) due to the stacking of peptides (Fig. 6c–f) during the self-assembly process. Electrical measurements were carried out by placing these fibrils on gold electrodes separated by a 300-nm non-conducting gap for two-probe and four-point probe measurements. Four-point probe measurements involve sending current through two outer probes while measuring voltage with two inner probes (Fig. 6g). This setup allows one to circumvent contact resistance during measurements.[68]

The two and four-point probe measurements demonstrated various conductivity values for each of the fibrils (Fig. 6h). The fibrils with metal and tyrosine, X1, demonstrated the highest conductivity of 3.5 ± 0.96 μS cm^{-1}. The fibril which contained no metal ions but contained the aromatic residues, X2, had conductivity values reduced sixfold to 0.59 ± 0.20 μS cm^{-1}. The fibrils, which contained no aromatic residues but contained metal ions, X3, had a conductivity of 0.11 ± 0.044 μS cm^{-1}, a value that is 32 times smaller than for X1. The fibril with neither aromatic residue nor metal ion, X4, did not assemble into lengths long enough to carry out four-point measurements but demonstrated a small two-probe conductivity of 0.35 ± 0.20 μS cm^{-1}. One of the points that was clear in the report is

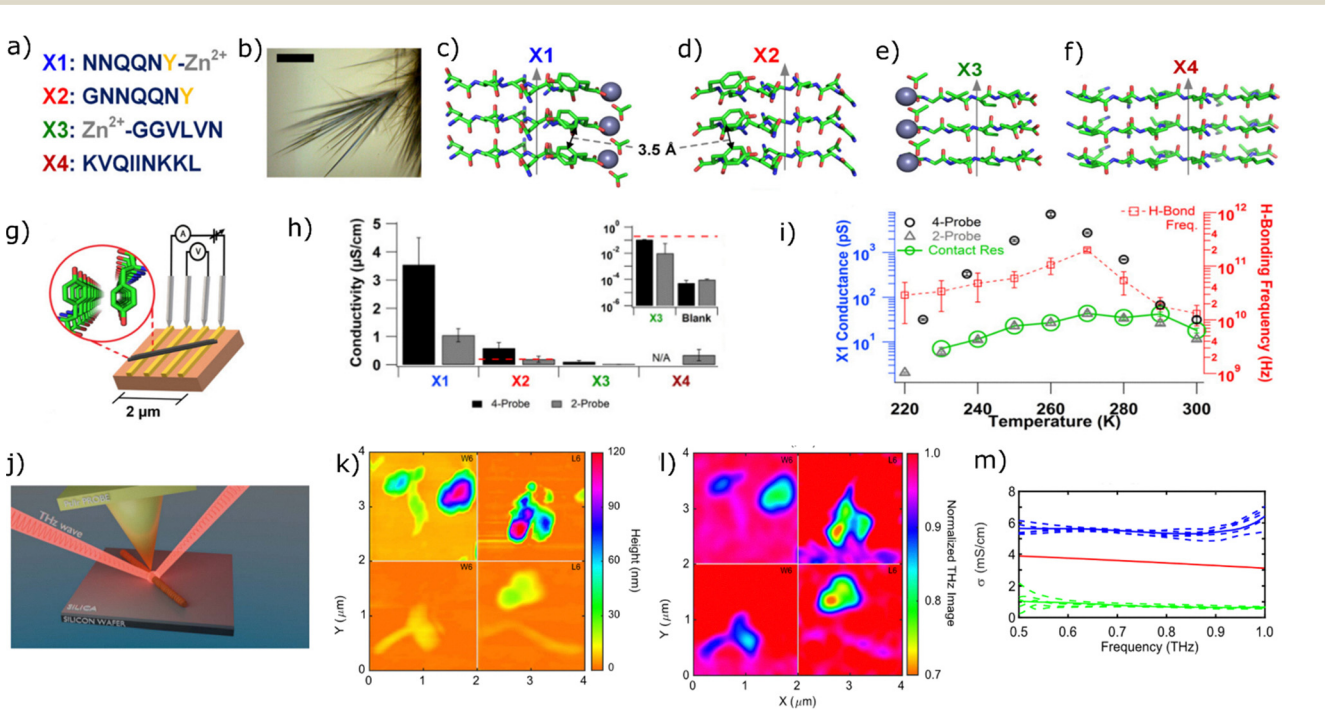

Fig. 6 (a) Sequence of amino acids prepared for the study with aromatic amino acid tyrosine (yellow) and zinc (grey). (b) Self-assembled amyloid fibril as seen under an optical microscope. (c)–(f) Molecular structure of the peptides in fibrils with the arrow pointing along the fibril axis. (g) Schematic of four-point measurement setup. (h) Two- and four-point probe conductivity of the fibrils. Inset shows zoomed-in values of response from X3 compared to blank electrodes. (i) Conductance of X1 fibrils as a function of temperature. Four-point probe measurement (black circle) demonstrates the role of temperature in conductance more clearly than the two-probe measurements (grey triangle), the values of which are similar to contact resistance (green circle).[67] Used in accordance with PNAS license from C. Shipps, H. R. Kelly, P. J. Dahl, S. M. Yi, D. Vu, D. Boyer, C. Glynn, M. R. Sawaya, D. Eisenberg, V. S. Batista and N. S. Malvankar, *Proc. Natl. Acad. Sci. USA*, 2021, **118**, e2014139118. Copyright 2021 Shipps *et al.* (j) Sketch of setup for THz response measurement with s-SNOM. (k) SNOM AFM topography image for aromatic amino acid-rich structures – W6 (left column) and aromatic amino acid-deficient structure – L6 (right column). (l) SNOM THz image normalized with respect to the silicon substrate for W6 (left column) and L6 (right column). (m) Conductivity of the W6 (blue) and L6 (green) peptide fibrils in THz regime compared with the conductivity of the silicon substrate (red).[69] Reprinted with permission from A. Solemanifar, X. Guo, B. C. Donose, K. Bertling, B. Laycock and A. D. Rakić, *Nanotechnology*, 2022, **33**, 065503. Copyright 2021 IOP Publishing Ltd.

that contact resistance in these systems can be significant enough that conductivity values acquired from the two-point probe measurements can be substantially different from the intrinsic conductivity (Fig. 6h). Two-probe measurements can also mask the transport properties, as demonstrated by the difference in the behaviour of temperature dependence of the conductance values from two-probe and four-point probe measurements (Fig. 6i).

The authors further carried out studies using molecular dynamics simulation and density functional theory calculation to understand the role of metal ions and aromatic residues in the fibrils. They observed that the role of metal ions in X1 was primarily to provide structural rigidity to the fibrils, thereby reducing the role of thermal fluctuations, allowing for more efficient electron transport along the length of the fibril. From the molecular dynamics simulations, it was observed that the tyrosine edge-to-edge distance was closer in the fibrils based on the peptides with metal ions, while the probability density of the electrons at the tyrosine edge-to-edge region for X2 was more spread out. This closer packing of the aromatic residues was suggested to be the reason for more effective electron transport along the fibril from X1 peptides.

Another method to circumvent the issue of contact resistance is to use non-contact-based techniques based on optical characterization. In 2022, A. Solemanifar *et al.*[69] carried out contact-free conductivity measurements on self-assembled aromatic amino acid-rich peptide fibrils using terahertz spectroscopy. The aromatic amino acid deficient peptide Ac–LHELA KLLHELAKLLKELAKL–NH_2 was inspired by the ones designed by Creasy *et al.*[65] It was named L6 and used as the negative control. The aromatic amino acid-rich peptide counterpart, labelled W6, had six leucine (L) at the hydrophobic core replaced by one of the aromatic amino acids, tryptophan (W).[70] The terahertz spectroscopy technique was used because its response is related to free carriers, unlike the responses in the mid and near-infrared regions, which are associated with resonances of bound carriers.[71]

Due to the large wavelength of about 300 μm at 1 THz and resulting diffraction limit, the resolution of terahertz imaging for nanoscale applications is challenging. The authors overcome this resolution limit by combining terahertz illumination with AFM-based scattering scanning near-field optical microscopy (s-SNOM, Fig. 6j), which allows for resolution to increase to hundreds of nanometres. According to this report, the combination of AFM-based s-SNOM with terahertz illumination increased the resolution to about 150 nm, a value much smaller than the wavelength of the terahertz signal. The sample was prepared by drop-casting solution with 200 μM peptide in PBS buffer onto silicon substrates. From the AFM topography image (Fig. 6k) and circular dichroism (CD) spectroscopy, it was observed that the self-assembly of both L6 and W6 peptides resulted in fibrillar structures with heights ranging anywhere from 10 nm to about 150 nm. Although the CD spectroscopy suggested that L6 fibrils had α-helical structures, it was estimated that W6 fibrils consisted of β-hairpin assemblies. The terahertz near-field contrast imaging (Fig. 6l) demonstrated that the aggregates of L6 and W6 fibrils were less reflective than the silicon substrate, with W6 fibril aggregates (Fig. 6l left panel) being more reflective than L6 fibril aggregates (Fig. 6l right panel). Based on the acquired calibrated reflectivity and phase from the THz measurements, the conductivity values of the samples were calculated for frequencies ranging from 0.5 to 1 THz (Fig. 6m). The conductivity values thus calculated were 5.7 ± 0.4 mS cm^{-1} for W6 fibrils and 0.7 ± 0.3 mS cm^{-1} for L6 fibrils. This observation, that W6 fibrils are about 8 times more conductive than the L6 sample, was in line with previous contact-based measurements carried out by Creasey *et al.*[61] This study further underscored the importance of aromatic residues in charge transport in peptide fibrils.

Structural basis for long-range electron transport

As discussed above, the reports of electron transport in self-assembled peptide fibrils have mostly been focused on demonstrating the relevance of aromatic amino acid residues for making electron transport possible. In the 2015 report from Creasy *et al.*, fluorescence spectroscopy and CD spectra were recorded to gain structural insight, which suggested that self-assembled fibrils demonstrated optical signals associated with closer packing of aromatic amino acids compared to the peptides that were not assembled into fibrils.[61]

In their 2018 study, Ing *et al.* suggested that the ACC-Hex fibrils they assembled did not show signs of π–π stacking. Yet their fibrils were capable of transporting electrons over distances of a few micrometers.[62] The self-assembled fibrils that this group constructed demonstrated not only Ohmic behaviour (Fig. 3e) but also that the conductivity of the fibrils increased with decreasing temperature (Fig. 3g). Typically, such temperature dependence of conductivity is attributed to delocalized electron transport (Fig. 7a) in metallic conductors, as opposed to thermally activated hopping (Fig. 7b), which requires an increase in temperature to promote charge transport. The control in their study, (Aβ)fibrils, had about 6 orders of magnitude lower conduction despite the presence of aromatic residues. The authors used this as a basis to suggest that a higher amount of electron conduction through ACC-Hex fibrils was not necessarily due to aromatic residues but due to the presence of α-helical backbone within the coiled-coil structure. The authors were not certain about the specific reason behind helicity causing such improvement in conductivity and suspected that the mechanism is possibly similar to the enhancement in conductivity observed in helical homopeptides due to helicity contributing to lowering the energy barrier and extending the electron cloud.[72]

While the role of the backbone in electron transport, as claimed by the authors, is entirely plausible since studies in short peptides have shown that helical backbone helps with electron transport,[72,73] comparing the conduction mechanism of ACC-Hex fibrils with Aβ fibrils is not necessarily fair. Aβ fibril assembly occurs through hydrogen bonding between the

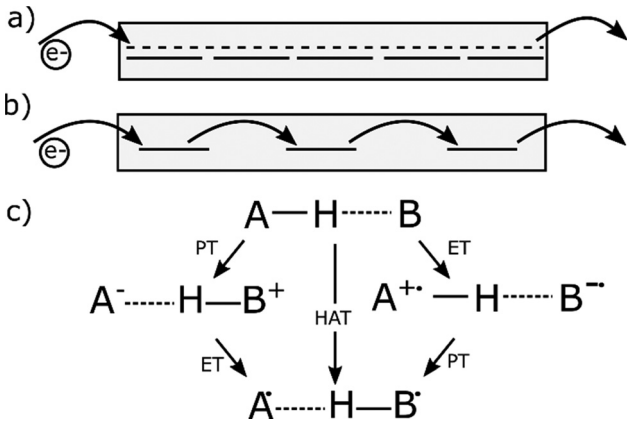

Fig. 7 Schematics of various electron transport mechanisms. (a) Delocalized electron transport due to close π–π overlap between electron-donating and accepting units. (b) Hopping transport, which requires electrons be provided with additional energy for them to be transported along the conducting chain. (c) One of the examples of proton-assisted electron transfer process, which involves a combination of proton transfer (PT) and electron transfer (ET) processes or direct hydrogen atom transfer (HAT) process. The list is not exhaustive of all the electron transport and transfer processes in peptides. Only the transport processes discussed in detail in the paper are represented.

β-strands, the density of aromatic residues in the hydrophobic core is smaller, and some of the aromatic residues form hydrophobic interaction pairs with non-aromatic units.[64] This suggests that the structure of Aβ fibrils is not conducive to making it possible for aromatic residues to be closely packed, unlike in the case of ACC-Hex fibrils, where most of the aromatic residues of the peptides are concentrated within the hydrophobic core of the fibrils.[63]

In their 2019 report, Creasey *et al.* investigated whether the self-assembled fibrils of aromatic amino acid-rich peptides that they had synthesized had substantial pi–pi stacking.[65] The fluorescence emission spectra of aromatic amino acid-rich F6 peptide fibrils demonstrated Stokes shift of the phenylalanine emission peak at 304 nm for F6 fibrils, which is attributed to π–π stacking. L6 fibrils did not show significant emission spectra. On the other hand, CD spectra demonstrated clear α-helical structures within L6 fibrils, while F6 fibrils demonstrated less stable α-helical structures with a potential mix of β-sheets, β-turns, or aggregates. In addition, their molecular dynamics simulation suggested that the inter-aromatic distance decreases over a longer timescale during assembly (Fig. 4i). However, the report did not have direct evidence of the confirmation of the aromatic residues in fibrils. Nevertheless, this report suggested that closer packing of aromatic residues is potentially a more important factor for long-range electron transport than the presence of helical backbones along the fibril length.

As in the case of the report by Creasey *et al.*, Shipps *et al.* also observed that the fibrils that were deficient in aromatic residues were less conducting than their counterpart with aromatic residues.[67] While other amino acids in peptides may participate in the electron transport, it was observed that stacked aromatic residues of tyrosine in their peptide fibrils substantially improved such transport. When comparing the fibrils composed of aromatic amino acids, the ones with tighter packing of aromatic residues displayed higher conductivity, further demonstrating the role of the aromatic sites in electron transport.

Most of these studies on long-range electron transport in self-assembled fibrils of peptides rich in aromatic amino acids are limited to the synthesis of peptides rich in aromatic residues and testing whether they are conducting. Mechanistic studies of electron transport in these systems are limited. One of the studies that stands out is the one reported by Shipps *et al.*,[67] in which experimental and computational studies have been carried out to understand the electron transport mechanism. The study reports that resistance of the fibrils increased linearly with fibril length, suggesting hopping transport (Fig. 7b) as the mechanism for electron transport. The conductance of the fibril increased as the temperature was lowered from 300 K to 260 K, but decreased when the temperature was further lowered to 220 K (Fig. 6i). Decreasing conductivity with decreasing temperature is consistent with thermally activated hopping transport. To understand the increase in conductivity while decreasing temperature at higher temperatures, the authors carried out molecular dynamics simulations, which suggested that the distance between aromatic residues did not change with temperature, but the probability of hydrogen bond formation between tyrosine hydroxyl–oxygen (Tyr–O) and glutamine amide–oxygen (Gln–O) increased by 15 fold when the temperature was reduced from 300 K to 270 k. Availability of proton-accepting units in facilitating the electron transfer process, called proton-coupled electron transfer (PCET) process, is one of the well-known mechanisms in biology.[74,75] All of these observations suggest that electron transport through these peptide fibrils results from the interplay between two thermally activated mechanisms: the availability of proton-accepting units through hydrogen bonds, which allows for proton-coupled electron transfer (Fig. 7c), and thermally activated hopping assisted by periodically spaced aromatic residues.

Lessons from electron transport in short peptides

As mentioned in earlier sections of this highlight, a considerable amount of work has been conducted on studying electron transport in individual short peptides and proteins, including attempts to understand the role of various molecular, chemical, and environmental factors in facilitating charge transport in those short peptides and proteins. Generally, electron transfer in short peptides occurs *via* tunnelling[2,76] as demonstrated by the dependence of electron transfer rate (k) with length (L) as $k \propto \exp(-\beta L)$, where β is the decay constant. Such a transport mechanism is vital in physiological processes involving energy conversion or storage. In these systems, electron transfer occurs up to distances of a few nanometres *via* tunnelling. However, such a tunnelling process cannot drive the electron

transport over long distances of tens of nanometres to micrometres.

However, there are reports of conduction through long peptides encompassing distances of tens of nanometres, which is considered ''long-range'' in the field of molecular electronics.[2,46] For instance, studying the conduction through proteins with lengths ranging from 4 to 20 nm by concatenating helix-turn-helix motif of CTPR proteins, a 2022 study by Zhang *et al.*[77] demonstrated that hopping transport, accompanied by lowering of reorganization energy, facilitated long-range transport in their molecular wires. Studies on such systems could be useful in understanding the possible mechanisms that enable long-range electron transport in the studies discussed herein.

Among some recent charge transport studies on short peptides and proteins, conductance studies in some peptide molecules have demonstrated that peptide bonds induce charge localization around them and therefore inhibit electron transport.[76] A 2024 study by Samajdar *et al.*[78] that combined a single-molecule experiment with molecular dynamics simulation to study conformations, and DFT theory to understand the charge transport mechanism, suggests that the conformation of the peptide is also an important factor in electron transport. Working with 4–5 amino acids, they observed that folded conformation, where the peptide could have a beta turn of 3_{10} helices, can allow for more efficient electron transport than an extended peptide. This observation that helical peptides promote electron transport compared to extended peptides is in line with other studies as well.[72,79] In the same study, the authors observed that the presence of H-bond, charges due to the zwitterionic state, and the presence of aromatic side-chain whose orbitals tend to mix well with the backbone orbitals can all contribute to enhancement in charge transport.

In 2023, Krishnan *et al.*[10] built an electron transfer model in conjunction with molecular dynamics simulations to understand previously reported fast electron transport in CTPR proteins with lengths up to 20 nm.[77] They suggested that the presence of aromatic residues in proteins can substantially lower the reorganization energy needed to overcome electron transfer between donor and acceptor sites. Previously, it has also been shown that electron transport in peptides can be facilitated by electron-rich sidechains such as alkene.[79] In fact, Ashkenasy *et al.* have demonstrated that adding cationic sidechains to insulating cyclic D,L-α-peptides can result in extended delocalization of electrons in self-assembled nanotubes of the peptide.[80] These observations underscore the importance of the electronic activities associated with residues and side chains in charge transport through peptides.

In principle, long-range charge transport in self-assembled peptide structures could be modelled as a series of sequential short-range electron transport.[5] However, in reality, the relative flexibility of peptide backbones, the presence of charges, the ability to construct intermolecular and intramolecular H-bonding, and the ability of aromatic residues to interact with other aromatic residues and peptide backbone result in peptide materials with electronic properties that are the result of the averaging of all these effects. Therefore, the observation of phenomena in molecules with a few amino acid units can not necessarily be generalized to molecules with a much longer amino acid sequence, let alone to the self-assembled supramolecular peptide fibrils, which are formed by multiple peptide units attached end-to-end with the help of various interactions effective over various ranges. This has been the bottleneck in the proliferation of research and development in peptide-based electronics, unlike the rapid growth in research and development in the field of organic electronic materials following the initial discoveries.

Where to go from here?

As mentioned above, the ultimate goal of all these efforts is to develop electron-conducting supramolecular assemblies of peptides for electronic applications. Conductive nanowires generated by *G. sulfurreducens*, which has been the inspiration for all the studies discussed above, have found applications in myriad electronic materials and devices, such as conductive composites,[81,82] memristors,[83] sensors,[84,85] and moisture gradient-based power generators.[86] Irrespective of their composition, nanowires generated by *G. sulfurreducens* are reported to have conductivity in the range of 20 mS cm^{-1}–30 S cm^{-1} (ref. 21) as calculated using two-probe measurements. The highest value of conductivity reported in the fibrils composed of self-assembled peptides rich in aromatic amino acids, thus far, is about 1 S cm^{-1}.[62] However, the conductivity values of fibrils from other such peptides are significantly lower, ranging from nS cm^{-1} to μS cm^{-1}, regardless of whether two-probe or four-point probe measurements were used (Table 1). The value of ~6 mS cm^{-1} reported by Solemanifar *et al.*[69] is also quite high; however, the measurement was carried out using optical techniques. For application in electronics, these materials would have to be placed between the electrodes, and therefore, the electron transport efficiency of these fibrils in such an arrangement is not clear.

A major achievement in the field would be to design peptides that can create supramolecular assemblies and consistently demonstrate conductivity of over tens of mS cm^{-1}. While this will not be enough to compete with organic electronic materials, which can have conductivity even in the range of thousands of S cm^{-1} and higher,[87] but given the ease of functionalization, ability to interact with ions, formation of hydrophilic shells, *etc.*, peptide-based electronic materials could find their use in sensing and bioelectronics.

Conductivity of a material (σ) is defined as:

$$\sigma = |e|nu$$

where, e is the charge of the mobile charge carrier (electron in this case), n is the carrier density, and u is the carrier mobility. It has been estimated[88] that carrier density of *G. sulfurreducens* nanowires is ~10^{20} cm^{-3} in par with organic conductors, and charge mobility in the order of ~10^{-4} cm^2 V^{-1} S^{-1}, a value similar to that of organic semiconductor a few decades ago, but a few orders lower than that of today's best-performing

Table 1 Summary of peptide fibrils developed for electron transport, including their dimensions, conductance or conductivity values whichever available, and type of sample and methods used for conductance measurements. Aromatic amino acids in the sequences are indicated in bold

Peptide sequence	Dimensions	Conductance (S) and/or conductivity (S cm^{-1})	Sample type	Measurement type
GF**P**R**FAG**F**P**[61]	Diameter: 0.4–0.6 nm Length: up to 10 μm	$\sim10^{-11}$ to 10^{-10} S (air) $\sim10^{-11}$ S (vacuum)	Fibril network	Two-probe (bridging electrodes) Electrode gap: 1 mm
ELKAIAQ**E**F**K**AIAKE**F**KA IA**F**^{I}E**F**KAIAQK[62]	Diameter: ~2 nm Length: ~10 μm	~5 mS	Fibril network	Two-probe (bridging electrodes) Electrode gap: 5 μm
		1.12 ± 0.77 S cm^{-1}	Individual fibril	Two-probe (bridging electrode-AFM tip)
FKE**F**AKL**F**KE**F**AKL**F**HE**F**AKL[65]	Diameter: ~3 nm Length: up to a few μm	$\sim10^{-9}$ S cm^{-1}	Fibril network	Two-probe (bridging electrodes) Electrode gap: 5 μm
AIPQ**F**SA**Y**RVKA**Y**NSAASSDLRNLKT ALESA**F**ADDQT**Y**PPES ($PilA_{19}$)[66]	Diameter: ~2 nm Length: ~6 μm	~1.1 nS	Individual fibril	Two-probe (bridging electrode-AFM tip)
Zn^{2+}NNQQN**Y**[67]	Diameter: ~188 nm Length: >50 μm	~3.5 μS cm^{-1}	Individual fibril	Four-point probe (bridging electrodes) Electrode gap: 300 nm
GNNQQN**Y**[67]	Diameter: ~76 nm Length: >50 μm	~0.59 μS cm^{-1}	Individual fibril	Four-point probe (bridging electrodes) Electrode gap: 300 nm
WHE**W**AKL**W**HE**W**AKL**W**KE**W**L[69,70]	Diameter: up to 20 nm Length: up to 4 μm	~6 mS cm^{-1}	Individual fibril	THz s-SNOM spectroscopy

organic semiconductors.[89] The studies on aromatic amino acid-rich peptide fibrils designed for electron conduction have not yet reported these conduction parameters. While conductivity is an important metric, getting insights into other charge transport parameters would help understand the current state and consider ways to improve them. Development of self-assembled peptide fibrils that have all these conduction parameters in the range demonstrated by *G. sulfurreducens* nanowires would mark a significant step to help proliferate this field.

Path forward

Current reductionist approaches, albeit slow and time-consuming, inspired by the role of various parameters on electron transport in short peptides, long peptides, and bio-based conducting proteinaceous nanowires, will continue to be a necessary step to advance this field. In the immediate and short term, more experimental studies of existing conducting systems and their derivatives, in conjunction with theoretical treatments and molecular dynamics simulations based on first principles, need to be carried out to develop a general sense of peptide sequences, their assembly into nanostructures, and roles of various aforementioned factors in electron transport. In the long run, the use of machine learning techniques as used in the design of various other supramolecular self-assemblies of peptides[90,91] could help accelerate the field. Developing a high-throughput machine learning model for predicting sequences of peptides whose supramolecular assemblies would allow for long-range electron transport is currently challenging due to limitations in the number of presently known peptide assemblies that have been identified for long-range electron transport.

There is no evolutionary pressure for most life on Earth to develop proteinaceous structures that enable long-range electron transport. Therefore, as discussed above, it was previously thought that proteins could not conduct over long distances. However, we now know that some microbes that survive in anaerobic environments do have evolutionary pressure to generate proteinaceous structures that can conduct over long distances to find electron acceptors in the surrounding and complete their metabolic cycle. The current body of work on developing electron conducting peptide-based supramolecular structures has been inspired by predicted structures of those proteinaceous filaments. Due to the diversity of amino acids and the number of ways they can fold, peptides best for creating assemblies that promote electron transport could be very different from biologically relevant peptides. The researchers in the field should be mindful that this, in turn, could induce bias in developing new sets of peptides for conduction and hence limit us from new discoveries.[91,92]

Combinatorial approaches within machine learning techniques could be a way to mitigate such bias. Rigid structures, helical backbones, higher density of aromatic amino acid residues, closer packing of the aromatic units, higher density of electron-rich sidechains, ability for H-bonds to assist with proton-coupled electron transfer, electrostatic screening of transport pathways, electron rich side chains, *etc.*, are some of the important parameters that are known to play role in making electron transport through peptide assemblies possible. By using these attributes to narrow down the possible combinations of amino acids in peptides and then working alongside experiments, breakthroughs may be realized.

Nevertheless, the ability to synthesize peptides with desired amino acid sequences allows pathways for one to engineer peptide units where all the contributions of constituent factors important in electron transport can be maximized, making efficient long-range electron transport possible. In addition, the need for peptide synthesis, structural analysis, charge transport measurements, molecular dynamic simulations, density functional theory calculations, and applying machine learning techniques demands that concerted interdisciplinary collaborations be carried out to gain deeper insights into understanding electron transport mechanisms in the self-assembled supramolecular structures of peptides rich in aromatic amino acids and move the field forward.

Conclusions

Over the past few decades, the ability to synthesize and engineer conducting organic molecules has allowed for the development of organic materials with a wide range of electronic, mechanical, and optical properties. As we look forward to sustainable alternatives for electronic materials with ease of functionalization, peptides and proteins could provide one possible alternative for developing such materials with varying electronic, optical, and mechanical properties. While the relative rigidity of π-conjugated backbones in organic electronic materials allows for precisely controlling their electronic properties, the flexibility of peptide bonds and therefore the ability of the peptides to conform in a multitude of ways makes it challenging to develop peptide-based electronic materials. However, various studies reported over the last decade and discussed herein have demonstrated that it is possible to design synthetic peptide sequences that can undergo self-assembly to form supramolecular fibrillar structures that can allow electron transport over long distances. This is encouraging, but there is still much groundwork to be done so that the conductivity of such fibrils can be further improved for broader application in electronics.

Author contributions

Ramesh Y. Adhikari – conceptualization, investigation, writing – original draft, review, and editing.

Conflicts of interest

There are no conflicts to declare.

Data availability

No primary research has been presented, and therefore, there is no data to share.

Acknowledgements

The author would like to thank Mark T. Tuominen from the Department of Physics and Derek R. Lovley from the Department of Microbiology at the University of Massachusetts Amherst, as well as Nikhil S. Malvankar from the Department of Molecular Biophysics and Biochemistry at Yale University for their mentorship and guidance during the author's time at University of Massachusetts Amherst. Furthermore, the author would like to thank the support from the National Science Foundation (NSF), Colgate University Start-up Fund, Colgate University Faculty Research Council, Eppley Foundation for Research, and Entrepreneurism, Policy, Innovation and Commerce (EPIC) at Jacksonville University over the years.

References

1 C. D. Bostick, S. Mukhopadhyay, I. Pecht, M. Sheves, D. Cahen and D. Lederman, *Rep. Prog. Phys.*, 2018, **81**, 026601.
2 N. Amdursky, D. Marchak, L. Sepunaru, I. Pecht, M. Sheves and D. Cahen, *Adv. Mater.*, 2014, **26**, 7142–7161.
3 T. Jiang, B.-F. Zeng, B. Zhang and L. Tang, *Chem. Soc. Rev.*, 2023, **52**, 5968–6002.
4 I. Ron, I. Pecht, M. Sheves and D. Cahen, *Acc. Chem. Res.*, 2010, **43**, 945–953.
5 N. L. Ing, M. Y. El-Naggar and A. I. Hochbaum, *J. Phys. Chem. B*, 2018, **122**, 10403–10423.
6 N. Amdursky, L. Sepunaru, S. Raichlin, I. Pecht, M. Sheves and D. Cahen, *Adv. Sci.*, 2015, **2**, 1400026.
7 S. Lindsay, *Life*, 2020, **10**, 72.
8 B. Zhang, W. Song, P. Pang, H. Lai, Q. Chen, P. Zhang and S. Lindsay, *Proc. Natl. Acad. Sci. U. S. A.*, 2019, **116**, 5886–5891.
9 B. Zhang, W. Song, J. Brown, R. Nemanich and S. Lindsay, *J. Am. Chem. Soc.*, 2020, **142**, 6432–6438.
10 S. Krishnan, A. Aksimentiev, S. Lindsay and D. Matyushov, *ACS Phys. Chem. Au*, 2023, **3**, 444–455.
11 M. Y. El-Naggar, G. Wanger, K. M. Leung, T. D. Yuzvinsky, G. Southam, J. Yang, W. M. Lau, K. H. Nealson and Y. A. Gorby, *Proc. Natl. Acad. Sci. U. S. A.*, 2010, **107**, 18127–18131.
12 S. Pirbadian, S. E. Barchinger, K. M. Leung, H. S. Byun, Y. Jangir, R. A. Bouhenni, S. B. Reed, M. F. Romine, D. A. Saffarini, L. Shi, Y. A. Gorby, J. H. Golbeck and M. Y. El-Naggar, *Proc. Natl. Acad. Sci. U. S. A.*, 2014, **111**, 12883–12888.
13 K. M. Leung, G. Wanger, M. Y. El-Naggar, Y. Gorby, G. Southam, W. M. Lau and J. Yang, *Nano Lett.*, 2013, **13**, 2407–2411.
14 S. Xu, A. Barrozo, L. M. Tender, A. I. Krylov and M. Y. El-Naggar, *J. Am. Chem. Soc.*, 2018, **140**, 10085–10089.
15 H. T. S. Boschker, P. L. M. Cook, L. Polerecky, R. T. Eachambadi, H. Lozano, S. Hidalgo-Martinez, D. Khalenkow, V. Spampinato, N. Claes, P. Kundu, D. Wang, S. Bals, K. K. Sand, F. Cavezza, T. Hauffman, J. T. Bjerg, A. G. Skirtach, K. Kochan, M. McKee, B. Wood, D. Bedolla, A. Gianoncelli, N. M. J. Geerlings, N. Van Gerven, H. Remaut, J. S. Geelhoed, R. Millan-Solsona, L. Fumagalli, L. P. Nielsen, A. Franquet, J. V. Manca, G. Gomila and F. J. R. Meysman, *Nat. Commun.*, 2021, **12**, 3996.
16 F. J. R. Meysman, R. Cornelissen, S. Trashin, R. Bonné, S. H. Martinez, J. van der Veen, C. J. Blom, C. Karman, J.-L. Hou, R. T. Eachambadi, J. S. Geelhoed, K. D. Wael, H. J. E. Beaumont, B. Cleuren, R. Valcke, H. S. J. van der Zant, H. T. S. Boschker and J. V. Manca, *Nat. Commun.*, 2019, **10**, 4120.
17 J. R. Van Der Veen, S. Hidalgo Martinez, A. Wieland, M. De Pellegrin, R. Verweij, Y. M. Blanter, H. S. J. Van Der Zant and F. J. R. Meysman, *ACS Nano*, 2024, **18**, 32878–32889.
18 R. Y. Adhikari, N. S. Malvankar, M. T. Tuominen and D. R. Lovley, *RSC Adv.*, 2016, **6**, 8354–8357.
19 Y. Tan, R. Y. Adhikari, N. S. Malvankar, J. E. Ward, T. L. Woodard, K. P. Nevin and D. R. Lovley, *mBio*, 2017, **8**, e02203-16.
20 M. J. Guberman-Pfeffer, N.-M. Dorval Courchesne and D. R. Lovley, *Nat. Rev. Bioeng.*, 2024, **2**, 869–886.
21 M. J. Guberman-Pfeffer, N.-M. Dorval Courchesne and D. R. Lovley, *Nat. Rev. Bioeng.*, 2024, **2**, 869–886.
22 D. R. Lovley and D. J. F. Walker, *Front. Microbiol.*, 2019, **10**, 2078.
23 D. R. Lovley, *Front. Microbiol.*, 2022, **13**, 872610.
24 F. Wang, Y. Gu, J. P. O'Brien, S. M. Yi, S. E. Yalcin, V. Srikanth, C. Shen, D. Vu, N. L. Ing, A. I. Hochbaum, E. H. Egelman and N. S. Malvankar, *Cell*, 2019, **177**, 361–369.
25 Y. Gu, M. J. Guberman-Pfeffer, V. Srikanth, C. Shen, F. Giska, K. Gupta, Y. Londer, F. A. Samatey, V. S. Batista and N. S. Malvankar, *Nat. Microbiol.*, 2023, **8**, 284–298.
26 S. E. Yalcin, J. P. O'Brien, Y. Gu, K. Reiss, S. M. Yi, R. Jain, V. Srikanth, P. J. Dahl, W. Huynh, D. Vu, A. Acharya, S. Chaudhuri, T. Varga, V. S. Batista and N. S. Malvankar, *Nat. Chem. Biol.*, 2020, **16**, 1136–1142.
27 F. Wang, K. Mustafa, V. Suciu, K. Joshi, C. H. Chan, S. Choi, Z. Su, D. Si, A. I. Hochbaum, E. H. Egelman and D. R. Bond, *Nat. Microbiol.*, 2022, **7**, 1291–1300.
28 N. S. Malvankar, M. Vargas, K. Nevin, P.-L. Tremblay, K. Evans-Lutterodt, D. Nykypanchuk, E. Martz, M. T. Tuominen and D. R. Lovley, *mBio*, 2015, **6**(2), e00084.

29 N. S. Malvankar, M. Vargas, K. P. Nevin, A. E. Franks, C. Leang, B.-C. Kim, K. Inoue, T. Mester, S. F. Covalla, J. P. Johnson, V. M. Rotello, M. T. Tuominen and D. R. Lovley, *Nat. Nanotechnol.*, 2011, **6**, 573–579.
30 S. Lampa-Pastirk, J. P. Veazey, K. A. Walsh, G. T. Feliciano, R. J. Steidl, S. H. Tessmer and G. Reguera, *Sci. Rep.*, 2016, **6**, 23517.
31 G. T. Feliciano, R. J. Steidl and G. Reguera, *Phys. Chem. Chem. Phys.*, 2015, **17**, 22217–22226.
32 D. J. F. Walker, R. Y. Adhikari, D. E. Holmes, J. E. Ward, T. L. Woodard, K. P. Nevin and D. R. Lovley, *ISME J.*, 2018, **12**, 48–58.
33 D. P. Baquero, V. Cvirkaite-Krupovic, S. S. Hu, J. L. Fields, X. Liu, C. Rensing, E. H. Egelman, M. Krupovic and F. Wang, *Cell*, 2023, **186**, 2853–2864.
34 T. Ueki, D. J. F. Walker, T. L. Woodard, K. P. Nevin, S. S. Nonnenmann and D. R. Lovley, *ACS Synth. Biol.*, 2020, **9**, 647–654.
35 K. Feron, R. Lim, C. Sherwood, A. Keynes, A. Brichta and P. Dastoor, *IJMS*, 2018, **19**, 2382.
36 L. Travaglini, N. T. Lam, A. Sawicki, H. Cha, D. Xu, A. P. Micolich, D. S. Clark and D. J. Glover, *Small*, 2024, **20**, 2311661.
37 L. Altamura, C. Horvath, S. Rengaraj, A. Rongier, K. Elouarzaki, C. Gondran, A. L. B. Maçon, C. Vendrely, V. Bouchiat, M. Fontecave, D. Mariolle, P. Rannou, A. Le Goff, N. Duraffourg, M. Holzinger and V. Forge, *Nat. Chem.*, 2017, **9**, 157–163.
38 Y. X. Chen, N. L. Ing, F. Wang, D. Xu, N. B. Sloan, N. T. Lam, D. L. Winter, E. H. Egelman, A. I. Hochbaum, D. S. Clark and D. J. Glover, *ACS Nano*, 2020, **14**, 6559–6569.
39 T. D. Rapson, T. D. Sutherland, J. S. Church, H. E. Trueman, H. Dacres and S. C. Trowell, *ACS Biomater. Sci. Eng.*, 2015, **1**, 1114–1120.
40 N. Amdursky, X. Wang, P. Meredith, D. J. Riley, D. J. Payne, D. D. C. Bradley and M. M. Stevens, *Adv. Mater.*, 2017, **29**, 1700810.
41 Y. Agam, R. Nandi, A. Kaushansky, U. Peskin and N. Amdursky, *Proc. Natl. Acad. Sci. U. S. A.*, 2020, **117**, 32260–32266.
42 O. Silberbush, M. Engel, I. Sivron, S. Roy and N. Ashkenasy, *J. Phys. Chem. B*, 2019, **123**, 9882–9888.
43 O. Silberbush, M. Amit, S. Roy and N. Ashkenasy, *Adv. Funct. Mater.*, 2017, **27**, 1604624.
44 M. Amit, S. Roy, Y. Deng, E. Josberger, M. Rolandi and N. Ashkenasy, *ACS Appl. Mater. Interfaces*, 2018, **10**, 1933–1938.
45 M. Amit, S. Appel, R. Cohen, G. Cheng, I. W. Hamley and N. Ashkenasy, *Adv. Funct. Mater.*, 2014, **24**, 5873–5880.
46 J. Jang and H. J. Yoon, *J. Am. Chem. Soc.*, 2024, **146**, 32206–32221.
47 N. Amdursky, *Curr. Opin. Electrochem.*, 2024, **47**, 101551.
48 S. Vishwakarma, O. S. Tiwari, R. Shukla, E. Gazit and P. Makam, *Chem. Soc. Rev.*, 2025, **54**(1), 465–483.
49 P. Chakraborty and E. Gazit, *ChemNanoMat*, 2018, **4**, 730–740.
50 Y. Wang, S. Rencus-Lazar, H. Zhou, Y. Yin, X. Jiang, K. Cai, E. Gazit and W. Ji, *ACS Nano*, 2024, **18**, 1257–1288.
51 C. Guo, Z. A. Arnon, R. Qi, Q. Zhang, L. Adler-Abramovich, E. Gazit and G. Wei, *ACS Nano*, 2016, **10**, 8316–8324.
52 M. S. Ekiz, G. Cinar, M. A. Khalily and M. O. Guler, *Nanotechnology*, 2016, **27**, 402002.
53 R. Y. Adhikari and J. J. Pujols, *Nano Select*, 2022, **3**, 1314–1320.
54 S. M. Acuña, M. C. Veloso and P. G. Toledo, *J. Nanomater.*, 2018, **2018**, 1–7.
55 V. Nguyen, R. Zhu, K. Jenkins and R. Yang, *Nat. Commun.*, 2016, **7**, 13566.
56 N. Hann-Deschaine, N. M. Viradia, J. J. Pujols, S. Miller and R. Y. Adhikari, *ACS Appl. Eng. Mater.*, 2024, **2**, 2219–2226.
57 L. Adler-Abramovich, D. Aronov, P. Beker, M. Yevnin, S. Stempler, L. Buzhansky, G. Rosenman and E. Gazit, *Nat. Nanotechnol.*, 2009, **4**, 849–854.
58 V. Basavalingappa, S. Bera, B. Xue, J. O'Donnell, S. Guerin, P.-A. Cazade, H. Yuan, E. U. Haq, C. Silien, K. Tao, L. J. W. Shimon, S. A. M. Tofail, D. Thompson, S. Kolusheva, R. Yang, Y. Cao and E. Gazit, *ACS Nano*, 2020, **14**, 7025–7037.
59 S. Bera, B. Xue, P. Rehak, G. Jacoby, W. Ji, L. J. W. Shimon, R. Beck, P. Král, Y. Cao and E. Gazit, *ACS Nano*, 2020, **14**, 1694–1706.
60 G. Finkelstein-Zuta, Z. A. Arnon, T. Vijayakanth, O. Messer, O. S. Lusky, A. Wagner, G. Zilberman, R. Aizen, L. Michaeli, S. Rencus-Lazar, S. Gilead, S. Shankar, M. J. Pavan, D. A. Goldstein, S. Kutchinsky, T. Ellenbogen, B. A. Palmer, A. Goldbourt, M. Sokol and E. Gazit, *Nature*, 2024, **630**, 368–374.
61 R. C. G. Creasey, Y. Shingaya and T. Nakayama, *Mater. Chem. Phys.*, 2015, **158**, 52–59.
62 N. L. Ing, R. K. Spencer, S. H. Luong, H. D. Nguyen and A. I. Hochbaum, *ACS Nano*, 2018, **12**, 2652–2661.
63 R. K. Spencer and A. I. Hochbaum, *Biochemistry*, 2016, **55**, 3214–3223.
64 T. Lührs, C. Ritter, M. Adrian, D. Riek-Loher, B. Bohrmann, H. Döbeli, D. Schubert and R. Riek, *Proc. Natl. Acad. Sci. U. S. A.*, 2005, **102**, 17342–17347.
65 R. C. G. Creasey, A. B. Mostert, A. Solemanifar, T. A. H. Nguyen, B. Virdis, S. Freguia and B. Laycock, *ACS Omega*, 2019, **4**, 1748–1756.
66 K. M. Cosert, A. Castro-Forero, R. J. Steidl, R. M. Worden and G. Reguera, *mBio*, 2019, **10**(6), e02721-19.
67 C. Shipps, H. R. Kelly, P. J. Dahl, S. M. Yi, D. Vu, D. Boyer, C. Glynn, M. R. Sawaya, D. Eisenberg, V. S. Batista and N. S. Malvankar, *Proc. Natl. Acad. Sci. U. S. A.*, 2021, **118**, e2014139118.
68 A. P. Schuetze, W. Lewis, C. Brown and W. J. Geerts, *Am. J. Phys.*, 2004, **72**, 149–153.
69 A. Solemanifar, X. Guo, B. C. Donose, K. Bertling, B. Laycock and A. D. Rakić, *Nanotechnology*, 2022, **33**, 065503.
70 A. Solemanifar, T. A. H. Nguyen, B. Laycock, H. M. Shewan, B. C. Donose and R. C. G. Creasey, *Mol. Syst. Des. Eng.*, 2020, **5**, 521–531.
71 L. Jung, J. Pries, T. W. W. Maß, M. Lewin, D. S. Boyuk, A. T. Mohabir, M. A. Filler, M. Wuttig and T. Taubner, *ACS Photonics*, 2019, **6**, 1744–1754.
72 L. Sepunaru, S. Refaely-Abramson, R. Lovrinčić, Y. Gavrilov, P. Agrawal, Y. Levy, L. Kronik, I. Pecht, M. Sheves and D. Cahen, *J. Am. Chem. Soc.*, 2015, **137**, 9617–9626.
73 N. Amdursky, *ChemPlusChem*, 2015, **80**, 1075–1095.
74 S. Y. Reece, J. M. Hodgkiss, J. Stubbe and D. G. Nocera, *Philos. Trans. R. Soc., B*, 2006, **361**, 1351–1364.
75 S. Y. Reece and D. G. Nocera, *Annu. Rev. Biochem.*, 2009, **78**, 673–699.
76 J. M. Brisendine, S. Refaely-Abramson, Z.-F. Liu, J. Cui, F. Ng, J. B. Neaton, R. L. Koder and L. Venkataraman, *J. Phys. Chem. Lett.*, 2018, **9**, 763–767.
77 B. Zhang, E. Ryan, X. Wang, W. Song and S. Lindsay, *ACS Nano*, 2022, **16**, 1671–1680.
78 R. Samajdar, M. Meigooni, H. Yang, J. Li, X. Liu, N. E. Jackson, M. A. Mosquera, E. Tajkhorshid and C. M. Schroeder, *Proc. Natl. Acad. Sci. U. S. A.*, 2024, **121**, e2403324121.
79 C. Guo, J. Yu, J. R. Horsley, M. Sheves, D. Cahen and A. D. Abell, *J. Phys. Chem. B*, 2019, **123**, 10951–10958.
80 N. Ashkenasy, W. S. Horne and M. R. Ghadiri, *Small*, 2006, **2**, 99–102.
81 Y.-L. Sun, H.-Y. Tang, A. Ribbe, V. Duzhko, T. L. Woodard, J. E. Ward, Y. Bai, K. P. Nevin, S. S. Nonnenmann, T. Russell, T. Emrick and D. R. Lovley, *Small*, 2018, **14**, 1802624.
82 J. M. Sonawane, E. Chia, T. Ueki, T. Woodard, J. Greener, S. S. Nonnenmann, J. Yao and D. R. Lovley, *Biosens. Bioelectron.*, 2025, **278**, 117378.
83 T. Fu, X. Liu, H. Gao, J. E. Ward, X. Liu, B. Yin, Z. Wang, Y. Zhuo, D. J. F. Walker, J. Joshua Yang, J. Chen, D. R. Lovley and J. Yao, *Nat. Commun.*, 2020, **11**, 1861.
84 X. Liu, T. Fu, J. Ward, H. Gao, B. Yin, T. Woodard, D. R. Lovley and J. Yao, *Adv. Electron. Mater.*, 2020, 2000721.
85 A. F. Smith, X. Liu, T. L. Woodard, T. Fu, T. Emrick, J. M. Jiménez, D. R. Lovley and J. Yao, *Nano Res.*, 2020, **13**, 1479–1484.
86 X. Liu, H. Gao, J. E. Ward, X. Liu, B. Yin, T. Fu, J. Chen, D. R. Lovley and J. Yao, *Nature*, 2020, **578**, 550–554.
87 M. B. Hasan, M. M. Parvez, A. Y. Abir and M. F. Ahmad, *Heliyon*, 2025, **11**, e42375.
88 R. Adhikari, PhD thesis, University of Massachusetts Amherst, 2016.
89 S. Fratini, M. Nikolka, A. Salleo, G. Schweicher and H. Sirringhaus, *Nat. Mater.*, 2020, **19**, 491–502.
90 F. Li, J. Han, T. Cao, W. Lam, B. Fan, W. Tang, S. Chen, K. L. Fok and L. Li, *Proc. Natl. Acad. Sci. U. S. A.*, 2019, **116**, 11259–11264.
91 M. Ramakrishnan, A. Van Teijlingen, T. Tuttle and R. V. Ulijn, *Angew. Chem.*, 2023, **135**, e202218067.
92 R. Batra, T. D. Loeffler, H. Chan, S. Srinivasan, H. Cui, I. V. Korendovych, V. Nanda, L. C. Palmer, L. A. Solomon, H. C. Fry and S. K. R. S. Sankaranarayanan, *Nat. Chem.*, 2022, **14**, 1427–1435.

